33rd Annual International Conference of the IEEE EMBS
Boston, Massachusetts USA, August 30 - September 3, 2011

Algorithms for Characterizing Brain Metabolites in Two-Dimensional *In Vivo* MR Correlation Spectroscopy

Daniel Cocuzzo, Alexander Lin, Saadallah Ramadan, Carolyn Mountford, Nirmal Keshava, *Member, IEEE*

Abstract—**Traditional analyses of *in vivo* 1D MR spectroscopy of brain metabolites have been limited to the inspection of one-dimensional free induction decay (FID) signals from which only a limited number of metabolites are clearly observable. In this article we introduce a novel set of algorithms to process and characterize two-dimensional *in vivo* MR correlation spectroscopy (2D COSY) signals. 2D COSY data was collected from phantom solutions of topical metabolites found in the brain, namely glutamine, glutamate, and creatine. A statistical peak-detection and object segmentation algorithm is adapted for 2D COSY signals and applied to phantom solutions containing varied concentrations of glutamine and glutamate. Additionally, quantitative features are derived from peak and object structures, and we show that these measures are correlated with known phantom metabolite concentrations. These results are encouraging for future studies focusing on neurological disorders that induce subtle changes in brain metabolite concentrations and for which accurate quantitation is important.**

I. Introduction

In this article, we introduce novel algorithmic approaches for processing and interpreting two-dimensional *in vivo* magnetic resonance spectroscopy measurements (MRS) collected using two-dimensional *in vivo* MR COrrelation SpectroscopY (2D COSY). Our effort uses a highly quantitative approach to decompose 2D COSY signals into constituent peak and object structures from which key features can be directly extracted. Our approach to interpreting 2D MRS signals differs from existing techniques that attempt to fit metabolite basis functions or presume the existence of a parametric, model-based signal structure.

The larger goal of our effort is to systematically and automatically derive features from 2D MRS that can be correlated with varying concentration levels of brain metabolites. MRS is already highly valued for its potential to quantitate chemical levels from data collected *in vivo*, but efforts in one-dimensional (1D) MRS have struggled to achieve this for a variety of reasons; ranging from repeatability of measurements to signal distortions that mitigate the effectiveness of model-based parameter estimation algorithms.

Manuscript received April 15, 2011. This work was supported by the IR&D program at the Charles Stark Draper Laboratory, the Harvard Catalyst Pilot Award, and the Department of Defense Grant W81XWH-10-1-0785.

Daniel Cocuzzo is with the Charles Stark Draper Laboratory, Cambridge, MA 02136 USA (phone: 617-258-4449; fax: 617-258-2772; email: dcocuzzo@draper.com).

Dr. Alexander Lin is with the Center for Clinical Spectroscopy at Brigham and Women's Hospital, Boston, MA 02120 (email: aplin@partners.org).

Dr. Saadallah Ramadan is with the Center for Clinical Spectroscopy at Brigham and Women's Hospital, Boston, MA (email: saad.ramadan@gmail.com).

Dr. Carolyn Mountford is with the Center for Clinical Spectroscopy at Brigham and Women's Hospital, Boston, MA 02120 (email: cmountford@partners.org)

Dr. Nirmal Keshava is with the Charles Stark Draper Laboratory, Cambridge, MA 02136 USA (e-mail: keshava@draper.com).

II. Background

In medicine, there continues to be a need for dramatic improvements in clinical care that lead to highly quantitative predictions, diagnosis, and treatments of disease states that are in line with increasing both the quality and efficiency of medical care. Supporting this objective is the ambitious goal of capitalizing upon the vast array of imaging technologies to obtain repeatable quantitative measures, biomarkers, that are accurate and free of human and machine bias. Technologies for which measurement capabilities can be made repeatable and consistently show the greatest promise of revolutionizing medical care by delivering high-quality medical treatment that is objective and accessible to all.

A. Magnetic Resonance Spectroscopy (MRS)

MR spectroscopy is the oldest of the molecular imaging modalities with the ability to perform in vivo interrogation of the chemistry of the human body. MRS of the brain permits non-invasive chemical analysis of the resting tissue state unavailable from traditional MR imaging (which only provides structural information) and fMRI (which provides hemodynamic information and requires a stimulus). MRS essentially provides the capability of a "virtual biopsy" of brain tissue from which estimates of metabolites, can enable a quantitative diagnosis of a wide array of disease states [1].

Specifically, MRS has been primarily used in the clinic for characterization and evaluation of brain tumors and associated treatments[2, 3]. MRS has also been shown to be diagnostic in Alzhiemer's disease, offering a pre-mortem diagnosis with high accuracy [4]. The American College of Radiology practice guidelines demonstrate over 20 different clinical applications of MRS [5]. Recently, MRS has also proven to be useful for the objective evaluation of traumatic brain injury [6] and chronic pain [7].

While this demonstrates the tremendous value of a non-invasive, objective, and quantitative virtual biopsy,

conventional 1D MRS is limited to the detection of 5-7 brain metabolites. This ultimately limits the sensitivity and specificity of the technique particularly in situations where co-morbidity of disease can cause changes to the same metabolite, such as trying to differentiate brain tumor from tumefactive multiple sclerosis which both exhibit similar spectral patterns [8].

A two-dimensional signal known as COrrelated SpectroscopY (2D COSY) is collected by using a simple two-pulse sequence (90x-t1-90x-Acq) at successive increments of T1, the delay between successive pulses. The advantage of 2D COSY is that is allows for the detection of up to 35 total brain metabolites. As with 1D MRS, a frequency transformation is typically applied to the signal to visualize spectral information, as shown in Figure 1.

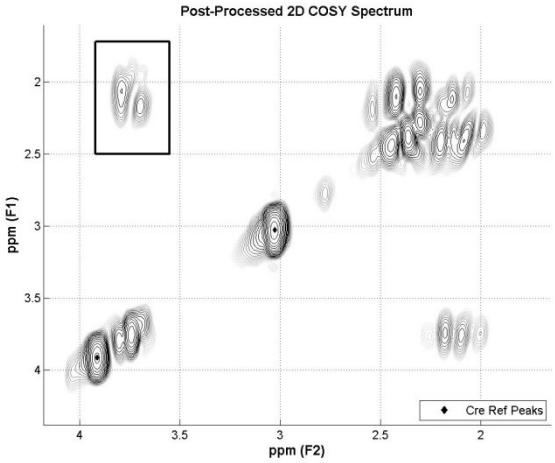

Fig. 1. A Post-Processed Phantom 2D COSY Spectrum

In a 2D COSY spectrum, a cross-peak indicates scalar coupling between the two protons it connects on the diagonal. It therefore allows for unambiguous resonance assignments for several metabolites. The novelty of the 2D COSY sequence is its ability to separate metabolites on a second level that may otherwise be indistinguishable using 1D MRS [9, 10] using the T2/F2 axis, and this has now been demonstrated in the human brain [11] [12] as well as brain tumors [13] and head injury [14].

Specifically, 2D COSY offers the ability for glutamine [2.10 ppm – 3.76 ppm] and glutamate [2.22 ppm - 3.73 ppm] cross-peaks to be separated (see highlighted region in Figure 1, with detail in Figure 2), which has not been possible in conventional 1D MRS. While some methods can isolate glutamate alone from a 1D spectrum, it is not possible to measure glutamate and glutamine together. Considering that the two metabolites are in rapid exchange through the glutamate-glutamine cycle, this is the first time that this cycle could be measured using proton spectroscopy with a conventional system.

B. 2D MRS Analysis Approaches

Analysis approaches for 2D MRS have primarily capitalized upon extensions of 1D approaches. The Felix NMR processing and analysis software package provides offline reconstruction of the COSY data which includes zero-filling, fourier transform of magnitude spectra in two dimensions, data filtration, and peak picking and chemical shift assignment[15]. Originally designed for high-resolution NMR spectra, the automated peak picking features do not perform well on *in vivo* data which necessitates manual peak selection and volume measurements. As a result, processing data using Felix is time- and labor-intensive and more importantly, highly user dependent. In contrast, the Pro-Fit package extends the 1D basis fitting approaches to 2D [16]. While this provides a more streamlined approach to 2D COSY cross-peak identification and quantitation, ProFIT is limited by the same constraints as other basis fitting approach which include the necessity of prior knowledge and unknown assumptions used when calculating metabolite measurements.

III. METHODS

A. Phantom Data Collection

For this analysis, a series of 2D MRS signals were obtained from seven unique phantom solutions containing glutamine (Gln), glutamate (Glu), creatine (Cre), and water. A Siemens TIM Trio 3T clinical MR scanner with a 12 element head coil was used for the collection of 2D Localized-COSY signals. An automated shim procedure was performed with manual adjustment to achieve a water peak line-width of at most 14 Hz. The WET weak water suppression procedure was applied at scan time to all collected signals. The resulting 2D COSY signals contain 96 increments of 0.8 ms along the T1 dimension, yielding an indirect spectral width of 1250 Hz, and 512 data points sampled along the T2 dimension with a spectral width of 2000 Hz. To improve SNR, each increment is computed as the average of eight repetitions.

The metabolite concentrations of the seven unique phantom solutions are shown in Table I. Creatine was held at a fixed concentration to serve as a reference for processing and analyses, whereas the concentrations of Gln and Glu were varied to investigate their 2D COSY spectral characteristics. The concentrations of metabolites used for this study are comparable to levels found in the human brain [17].

TABLE I
Metabolite Concentrations of Phantom Scans

Metabolite Concentration (mM)	Phantom ID 1	2	3	4	5	6	7
Glutamine (Gln)	6	6	12	6	3	12	3
Glutamate (Glu)	12	18	12	6	12	18	6
Creatine (Cre)	10	10	10	10	10	10	10

B. 2D COSY Post-Processing Techniques

A suite of tools was developed by C.S. Draper Laboratory to handle the extraction of raw COSY data, in addition to post-processing techniques to mitigate artifacts introduced during data collection. The raw COSY signals are zero-filled in both the T1 and T2 dimensions to increase spectral resolution in the frequency domain, yielding COSY signals that are [576 x 2048] data points in size. A two-dimensional shifted sine bell apodization function is applied to simultaneously reduce the dominant water resonance and accentuate metabolites of interest. In MRS, data is commonly visualized as a spectrum in the frequency domain with a corresponding unit-less parts-per-million (ppm) axis that is independent of acquisition parameters. We perform a two-dimensional Fourier transform and use the stable Cre reference at known locations [3.027 ppm and 3.913 ppm] to generate reference axes for visualization. The reference axes allow approximate identification of diagonal and cross-peak metabolite resonance structures that have been empirically reported in the MRS literature [18], such as those shown in Figure 2.

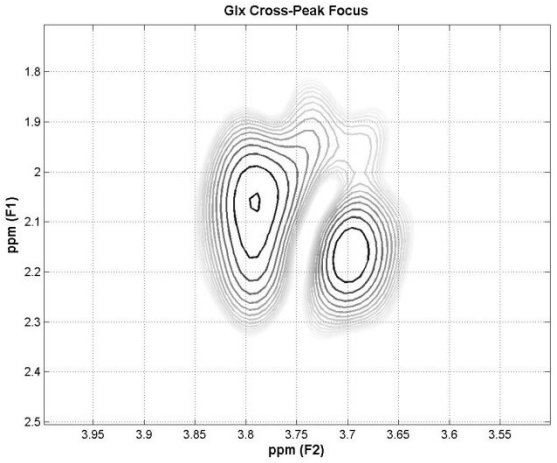

Fig. 2. An Example of Glx Cross-Peak Spectral Focus for a Post-Processed Phantom Scan

C. NIWVF Peak Detector

The peak detector we use is a variant of the Intensity Weighted Variance Filter originally derived for chemometric signals [19] that identifies a peak in a windowed interval having W points centered around time index value, k, of a discrete time series $y(k)$, by calculating a test statistic, $s^2(k)$, indicative of the weighted variance of points within an interval around a center time point, k:

$$s^2(k) = \frac{\sum_{j=k-W/2}^{k+W/2} y(j)(x(j)-k)^2}{\sum_{j=k-W/2}^{k+W/2} y(j)}. \qquad [1]$$

The premise of the detector is that estimates of local, weighted variance will differ when a peak-like structure is present. This value was normalized by the corresponding variance of a uniform distribution over the same interval

$$\sigma_U^2 = \frac{(W+1)(W-1)}{12} \qquad [2]$$

and $\frac{s^2(k)}{\sigma_U^2}$ was used in a hypothesis test that tests for the presence of peaks by comparing the locally-calculated variance with that expected from an interval having no peak (i.e., a uniformly distributed interval). Our implementation used the normalized IWVF (NIWVF) [20], created by amending the IWVF to include a normalizing factor that penalizes peak structures having extremely small values:

$$w(k) = \frac{s^2(k)-\sigma_U^2}{\left(\frac{\sigma_U^2}{\overline{y}_{W(k)}}\right)+a_0}, \qquad [3]$$

where $\overline{y}_W(k)$ is the average value of $y(k)$ over the windowed interval of interest, and a_0 is a penalty factor that adjusts standard errors towards a common value. We let $a_0 = 0$ in our analyses.

Using the values traced out by $w(k)$, the centers of peaks were detected at the minimum values of $w(k)$. This process was repeated for a range of relevant window lengths which typically finds the minimal window length that compactly encloses a peak. For our analyses, the window widths were chosen to be from 5 to 21 spectral points along the T2/F2 dimension, and at each point, the lowest value of $w(k)$ was retained along with the corresponding window width that induced it. To enable reliable and predictable detection of peaks, a closed-form theoretical relationship was derived for each window length relating a threshold value for $w(k)$ to the expected Probability of False Alarm and Probability of Detection rates for peaks, based on empirically derived estimates of noise mean and variance. These expressions relating thresholds to expected peak detection performance capitalized upon the fact that the predicted statistical distributions for $w(k)$ are Gaussian, regardless of whether a peak is actually present. However, in reality, peak structures are often asymmetric, causing the minima of $w(k)$ to be slightly offset from the location of the true peak value of chemical structures. Consequently, a correction algorithm introduced minor adjustments to ensure the accurate location of the peak maximum value.

Our algorithm employs the NIWVF serially along each

row (F2 dimension) to identify the location and width of peaks in each row. Utilizing the detected peaks from all rows, distinct chemical object structures were demarcated across rows through connectivity rules that are commonly used in computer vision. Unconnected peaks were eliminated, resulting in a binary map for the entire signal. Chemical peak and object parameters were subsequently derived from each distinct chemical structure and correlated with diagonal and off-diagonal cross-peak resonances.

D. *Quantitative Features for Chemical Structures*

In order to compare the peak and object structures obtained across all phantom scans, a set of quantitative features were extracted from each scan. These features are natural extensions of the peak and object detection algorithms and facilitate quantifying the changing 2D COSY spectral resonance structures as a function of different metabolite concentrations in the phantom solutions. The features are:

- The number of detected peaks
- The sum of the spectral intensities of all detected peaks
- The maximum spectral intensity of a detected peak
- The number of detected object structures
- The sum of the spectral intensities within the area spanned by all detected object structures
- The maximum spectral intensity within the area spanned by a single object structure

IV. Results & Discussion

A. *Detection of Peaks and Objects*

We focused this analysis on a spectral window of [1.72 ppm – 2.5 ppm] in the T1/F1 direction, and [3.55 ppm – 3.92 ppm] in the T2/F2 direction; inspection of MRS literature tells us that this spectral window contains the cross-peaks associated with intra-molecular interactions, revealed by 2D COSY [18]. Peak detection and object segmentation was performed within this spectral focus window to specifically investigate spectral characteristics of Gln and Glu cross-peak structures. Sample results from the peak and object segmentation algorithms applied to the spectral region appearing in Figure 2 are shown in Figure 3 and Figure 4, respectively. These figures indicate the locations of detected peaks and constructed objects, but omit spectral intensity information, from which the features previously discussed are derived.

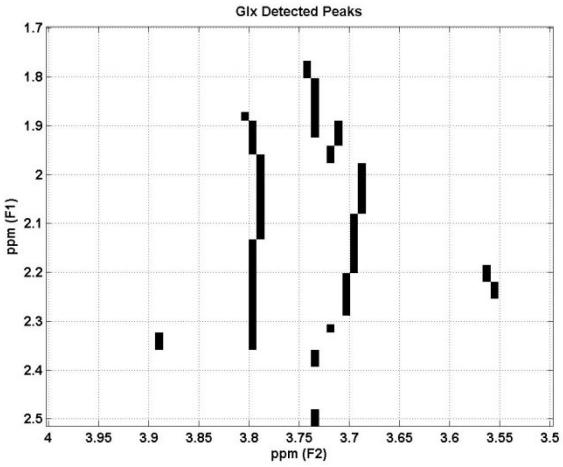

Fig. 3. An Example of the Detected Peak Structures of a Phantom Scan

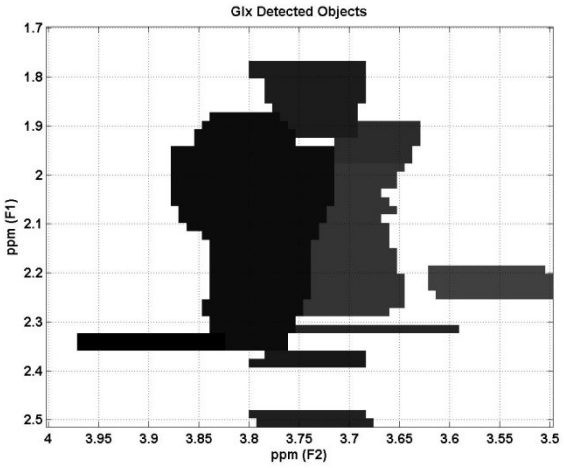

Fig. 4. An Example of the Detected Object Structures of a Phantom Scan

B. *Linear Correlations with Metabolite Concentrations*

In order to investigate the effects of changing the concentration of a single metabolite on the derived quantitative metrics, we chose subsets of the phantom scans for which one of the metabolites of interest (Gln/Glu) was held constant. The selected phantom scans correspond to the highlighted cells in Table I; the row label indicates the metabolite of interest, whereas the highlighted cells indicate which scans are used. Note that the other metabolite (Glu/Gln) is held at a constant concentration. This allows our analysis to focus on spectral changes due to the variation of the concentration of a single metabolite only. However, this reduces the number of appropriate data points available for correlation.

For each of the quantitative metrics described above, we performed three linear correlations; with the concentration of Gln (Glu held constant), with the concentration of Glu (Gln held constant), and with the concentration of Glx. Glx is defined as the sum of the concentration of Gln and Glu for a phantom scan. Figure 5 shows the plots of Glu/Gln/Glx

metabolite concentrations versus the maximum spectral intensity of a detected peak across the spectral focus window. The linear regression function is overlaid to indicate the strong relationship between concentration and intensity values, most prominently for Glx. Although here we show correlations corresponding to a single feature only, this process was applied to each of the quantitative feature previously discussed.

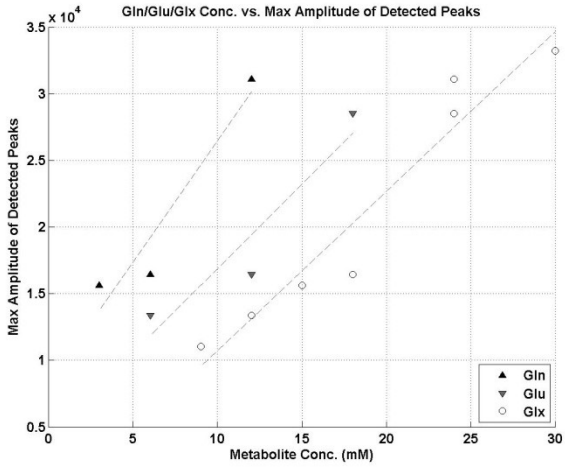

Fig. 5. Gln/Glu/Glx Concentrations vs. Maximum Spectral Intensity of Detected Peaks

From the linear correlations, we obtain the correlation coefficient, R, and the p-value that indicates the likelihood of a relationship between the two variables of interest. The results of all linear correlations are tabulated in Table II and Table III, showing the correlation coefficients and p-values respectively.

Table II
Computed Linear Correlation Coefficients (R)

Correlation Coefficient, R	Gln	Glu	Glx
Number of Peaks	1.000	0.693	0.838
Sum of Peak Vals	0.944	0.893	0.962
Max Peak Val	0.959	0.946	0.966
Number of Objects	0.500	0.866	0.899
Sum of Object Areas	0.959	0.901	0.962
Max Object Area	0.927	0.855	0.954

Table III
Computed Linear Correlation P-Values

P-value	Gln	Glu	Glx
Number of Peaks	**0.000**	0.512	**0.019**
Sum of Peak Vals	0.215	0.298	**0.001**
Max Peak Val	0.183	0.211	**4.1E-04**
Number of Objects	0.667	0.333	**0.006**
Sum of Object Areas	0.184	0.286	**0.001**
Max Object Area	0.244	0.347	**0.001**

Although the correlations between the quantitative metrics and the concentrations of Gln and Glu achieve high correlation coefficients R, the associated p-values are undesirably high due to the limited number of available data points. This does not detract from our technique, and we expect improvement in applications with a greater number of data samples, such as the improvements in correlation significance of Glx versus Glu/Gln. As Table II and Table III indicate, the correlations involving Glx perform quite well across all of the derived metrics; the strongest association was found between the concentration of Glx and the maximum spectral intensity of a detected peak structure within the spectral focus window.

V. Conclusions

2D COSY offers a unique opportunity to observe the results of metabolic processes in the brain and offers spectral information that is not easily resolved by traditional 1D MRS. In particular, subtle changes in the concentrations of Gln/Glu/Glx can provide significant insight into the processes accompanying key disorders such as mTBI, PTSD, CTE, and chronic pain.

Our current approach exhibits flexibility in characterizing complex diagonal and cross-peak resonance structures found in *in vivo* 2D COSY spectra. Our technique avoids the limitations of strict adherence to model-based approaches, where performance is not always reliable due to the quality of real-world data, making it attractive for *in vivo* studies. We hope to extend this approach for neurological disorders, such as those mentioned above.

Additional work needs to be done to more accurately identify and segment distinct metabolite resonances, but a framework has been constructed to precisely excise key structures in 2D COSY that can be used for distinguishing similar metabolites, and ultimately to quantitate specific chemical concentrations. Future articles will document the results of applying automated algorithms to 2D MRS signals generated from phantoms as well as from humans.

Acknowledgment

The authors would like to acknowledge Dr. Martin Svedlow at Draper Laboratory for the development of the NIWVF peak detector, Hayden Box for the phantom construction and data collection, and Dr. Albert Thomas and Dr. Gaurav Verma at the UCLA Department of Radiology for providing software for reading 2D MRS signals.

References

[1] Mountford, C.E., et al., *Neurospectroscopy: The Past, Present, and Future.* Chem. Rev., 2010. **110**(5): p. 3060-3086.

[2] Lin, A.P., S. Bluml, and A.N. Mamelak, *Efficacy of Proton Magnetic Resonance Spectroscopy Inclinical Decision Making for Patients with Suspected Malignant Brain Tumors.* Journal of Neuro-Oncology, 1999. **45**(1): p. 69-81.

[3] Hollingworth, W., et al., *A Systematic Literature Review of Magnetic Resonance Spectroscopy for the Characterization of Brain Tumors.* American Journal of Neuroradiology, 2006. **27**(7): p. 1404-1411.
[4] Kantarci, K. and C.R. Jack, *Quantitative Magnetic Resonance Techniques as Surrogate Markers of Alzheimer's Disease.* NeuroRx, 2004. **1**(2): p. 196-205.
[5] *ACR-ASNR Practice Guideline for the Performance and Interpretation of Magnetic Resonance Spectroscopy of the Central Nervous System.* 2008.
[6] Lin, A.P., et al., *Neurochemical Changes in Athletes with Chronic Traumatic Encephalopathy.* Radiological Society of North America, 2010.
[7] Stanwell, P., et al., *Neuro magnetic resonance spectroscopy using wavelet decomposition and statistical testing identifies biochemical changes in people with spinal cord injury and pain.* NeuroImage, 2010. **53**(2): p. 544-552.
[8] Saindane, A.M., et al., *Proton MR Spectroscopy of Tumefactive Demyelinating Lesions.* American Journal of Neuroradiology, 2002. **23**(8): p. 1378-1386.
[9] Ramadan, S. and C.E. Mountford, *Two-Dimensional Magnetic Resonance Spectroscopy on Biopsy and In Vivo.* Annual Reports on NMR Spectroscopy, 2009. **65**: p. 161-199.
[10] Ryner, L.N., J.A. Sorensen, and M.A. Thomas, *Localized 2D J-Resolved 1H MR Spectroscopy: Strong coupling effects In Vitro and In Vivo.* Magnetic Resonance Imaging, 1995. **13**(6): p. 853-869.
[11] Thomas, M.A., et al., *Localized Two-Dimensional Shift Correlated MR Spectroscopy of Human Brain.* Magentic Resonance in Medicine, 2001. **46**(1): p. 58-67.
[12] Ziegler, A., et al., *Localised 2D Correlation Spectroscopy in Human Brain at 3T.* Magn Reson Mater Phy 2001. **14**: p. 45-49.
[13] Ramadan, S., et al., *Use of in Vivo Two-dimensional MR Spectroscopy to Compare the Biochemistry of the Human Brain to That of Glioblastoma.* Radiology, 2011.
[14] Lin, A.P., et al., *In Vivo L-COSY Identifies Neurochemical Changes in Professional Athletes with Repetitive Head Injuries.* Proc. Intl. Soc. Mag. Reson. Med, 2011.
[15] *Felix 2D/ND NMR Software.* http://www.felixnmr.com/felix2dnd.htm
[16] Schulte, R.F. and P. Boesiger, *ProFit: two-dimensional prior-knowledge fitting of J-resolved spectra.* NMR in Biomedicine, 2006. **19**: p. 255-263.
[17] Kreis, R., T. Ernst, and B.D. Ross, *Absolute Quantitation of Water and Metabolites in the Human Brain. II. Metabolite Concentrations.* Journal of Magnetic Resonance, 1993. **102**(1): p. 9-19.
[18] Govindaraju, V., K. Young, and A.A. Maudsley, *Proton NMR chemical shifts and coupling constants for brain metabolites.* NMR in Biomedicine, 2000. **13**: p. 129-153.
[19] Jarman, K.H., et al., *A new approach to automated peak detection.* Chemometrics and Intelligent Laboratory Systems, 2003. **69**: p. 61-76.
[20] Willse, A., et al., *Identification of Major Histocompatibility Complex-Regulated Body Odorants by Statistical Analysis of a Comparative Gas Chromatography/Mass Spectrometry Experiment.* Analytical Chemistry, 2005. **77**: p. 2348-2361.